ARTICLE

Potentiometric *in Situ* Monitoring of Anions in the Synthesis of Copper and Silver Nanoparticles Using the Polyol Process

Jesse L. Carey, III,[†] David R. Whitcomb,[‡] Suyue Chen,[†] R. Lee Penn,[†] and Philippe Bühlmann*[,†]

[†]Department of Chemistry, University of Minnesota, 207 Pleasant Street SE, Minneapolis, Minnesota 55455, United States and [‡]Carestream Health, 1 Imation Way, Oakdale, Minnesota 55128, United States

ABSTRACT Potentiometric sensors, such as polymeric membrane, ion-selective electrodes (ISEs), have been used in the past to monitor a variety of chemical processes. However, the use of these sensors has traditionally been limited to aqueous solutions and moderate temperatures. Here we present an ISE with a high-capacity ion-exchange sensing membrane for measurements of nitrate and nitrite in the organic solvent propylene glycol at 150 °C. It is capable of continuously measuring under these conditions for over 180 h. We demonstrate the usefulness of this sensor by *in situ* monitoring of anion concentrations during the synthesis of copper and silver nanoparticles in propylene glycol using the polyol method. Ion chromatography and a colorimetric method were used to independently confirm anion concentrations measured *in situ*. In doing so, it was shown that in this reaction the co-ion nitrate is reduced to nitrite.

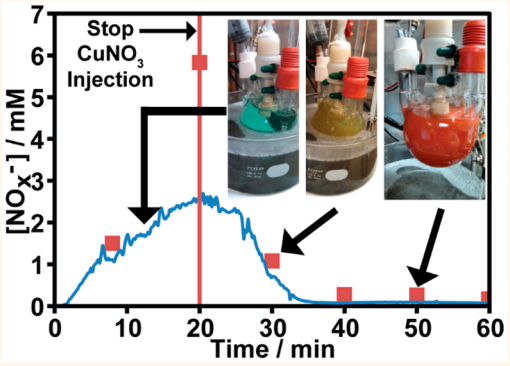

KEYWORDS: polyol · silver nanoparticles · copper nanoparticles · *in situ* monitoring · ion-selective electrodes · nitrate · nitrite

Silver nanoparticles have found use in a wide range of applications, such as in catalysis,[1,2] electronics,[3,4] electrochemical sensors,[4] surface-enhanced Raman spectroscopy (SERS),[5] optics,[4,6] printable conducting inks,[7] antimicrobials,[8] and bioimaging.[9] Although less popular, copper nanoparticles are also the focus of growing interest, and uses are found in areas such as printable conducting inks, where the combination of similar conductivity but lower cost gives copper an advantage over silver nanoparticles.[10] These nanoparticles are often synthesized using the polyol process, which permits the control of the nanoparticle size and shape.[11−15] In these reactions, propylene glycol and ethylene glycol are used both as the solvent and the reagent to reduce the metal ions.[13] The more viscous the solvent, the smaller and narrower the size distribution of the particles.[13] Importantly, these reactions are often performed at temperatures near 150 °C because the reducing strength of these polyols increases with temperature, possibly as a result of the formation of aldehyde derivatives at high temperatures.[14,16] The higher the temperature, the faster the reaction rate and the smaller the average particle size.[12] However, much about the mechanism of this reaction is still unknown, including the extent to which anions affect the size and shape of the nanoparticles.

Silver nitrate is commonly used in the synthesis of silver nanoparticles,[14] while copper nitrate has only been used a few times to synthesize copper nanoparticles.[12,15] Nitrate may be reduced by aldehydes, which form in glycols at high temperatures.[17] In acidic environments, nitrate may also oxidize silver particles back into $AgNO_3$, with $NO_{(g)}$ as a byproduct.[17,18] The effect of HNO_3 on silver nanoparticles is referred to as oxidative etching and can have dramatic effects on the shape and size distribution of nanoparticles.[19] The addition of NO_2 affects the shape of Pt/Pd nanoparticles, which has been hypothesized to result from interactions between NO_2 and the nanoparticle surface.[20]

* Address correspondence to buhlmann@umn.edu.

Received for review August 18, 2015 and accepted November 18, 2015.

Published online November 18, 2015
10.1021/acsnano.5b05170

For a better understanding of the parameters controlling nanoparticle synthesis, it is desirable to perform *in situ* monitoring of the chemical species that are formed or decomposed. *In situ* techniques that have been used for this purpose include UV−visible spectroscopy,[21] redox potential measurements,[22,23] small-angle X-ray scattering (SAXS),[24] and dispersive X-ray absorption spectroscopy (DXAS),[25] but these techniques have only allowed for the observation of structural changes by nanoparticles during their synthesis. To expand the range of techniques available for *in situ* monitoring of the polyol synthesis of nanoparticles, we explored the use of ion-selective electrodes (ISEs). The ability of ISEs to monitor ion activities *in situ*, without the inconvenience associated with sampling, is a major advantage, compared to methods of analysis that require the removal of aliquots from the reaction, such as colorimetric testing or ion chromatography. Sampling and sample workup can introduce artifacts, and *ex situ* techniques are often not able to distinguish between freely dissolved ions and ions that are either bound in the form of a complex or are adsorbed to the nanoparticle surface. *In situ* monitoring with potentiometric sensors has been demonstrated, *e.g.*, in clinical chemistry,[26] in environmental studies,[27] or to assess the toxicological effects of silver nanoparticles on bacteria.[28] However, most of this work was performed in aqueous systems, with only few reports of measurements in water/alcohol mixtures (usually with less than 50% alcohol).[29−32] The use of many ISEs in organic media is limited by leaching of the ionophore, ionic sites, and plasticizer out of the polymeric sensing membranes into the analyzed liquid. Also, little work has been performed at high temperatures, where plasticized polymeric sensing membranes have a reduced mechanical strength. Most plasticized polymer electrodes can only be used for work up to 50 °C, although the use of some plasticized polymer electrodes at slightly higher temperatures was reported.[33,34] ISEs have previously been used to monitor the concentration of silver ions during the room temperature synthesis of silver nanoparticles in aqueous solutions by hydroquinone-induced precipitation of silver onto gold nanoparticle seeds. However, it appears unlikely that the sensors used for that work would be able to function in the harsh conditions of the polyol process since weakening of the non-cross-linked polyacrylate membrane at high temperatures and leaching of membrane components into the hot organic solvent would be expected.[35]

We are demonstrating here the use of hydrophilic, high-capacity ion-exchange membranes (more commonly used in electrodialysis, fuel cells, and batteries)[36] as ISE sensing membranes that can function not only in aqueous samples but also in organic solvents and at high temperatures. Anion-exchange resins were first developed in the 1930s for ion-exchange separations,[37] and they have been used in organic solutions with relatively high dielectric constants.[38] ISEs with resin-based, ion-exchange membranes were used to measure ion concentrations in aqueous samples as early as the 1950s[39,40] and also found applications for measurements in liquid ammonia and ethanol.[41] More recently, Bakker and co-workers showed that commercially available hydrophilic ion-exchange membranes can be used to prepare potentiometric ion sensors for the measurement of chloride in blood.[42]

Most modern high-capacity ion-exchange membranes consist of a highly cross-linked polymer to which ion exchange sites (often referred to as ionic sites) are covalently attached. Unlike many conventional ion-exchange ISE membranes, they do not contain a plasticizer.[38] Therefore, we expected that hydrophilic high-capacity ion-exchange membranes would suffer less from exposure to organic solvents. Moreover, the high level of cross-linking that is common in commercial high-capacity ion-exchange membranes and the absence of a plasticizer was expected to provide the membranes with sufficient mechanical strength even at high temperatures. Ion-exchange membranes with a high ion-exchange capacity are thought to contain nanometer-scale pores or channels with high charge density,[36,43] the size of which varies with the degree of cross-linking.[38] Ion transport through these membranes has been described as occurring through nanopores,[44,45] which are filled with the solvent with which the membrane is in contact. In this regard, ISEs with high-capacity ion-exchange membranes resemble the recently developed sensors based on porous gold films with nanopores that are made to be permselective by charged species that are immobilized on the gold surface.[46,47] Because the state of solvation of the exchangeable ions is very similar in these nanopores and within the sample solutions, high-capacity ion-exchange membranes without ionophores exhibit a very narrow range of selectivity,[42] quite in contrast to hydrophobic ion-exchange membranes with a low ion-exchange capacity and low dielectric constant.[48]

RESULTS AND DISCUSSION

Effect of High Temperature Exposure on Subsequent ISE Performance at Room Temperature. Three types of hydrophilic, high-capacity ion-exchange membranes were used in this work, *i.e.*, Fumasep FAB,[49] SELEMION AHO,[50] and AMI-7001S anion-exchange membranes.[51] While these three types of ion-exchange membranes differ somewhat in the way they are manufactured, they all have a thickness between 0.1 and 0.5 mm, show good permselectivity, and have a low electrical resistance (<40 Ω cm^{-2}). They were selected from among many commercially available anion-exchanger membranes because their manufacturers reported that they were suitable for use at higher temperatures. While only

the manufacturers of the SELEMION AHO and AMI-7001S membranes specifically identified the ion-exchanger sites as quaternary ammonium groups, the same is likely true for the Fumasep FAB membranes.

All anion-exchange membranes were first immersed into a 0.5 M sodium nitrate solution in propylene glycol for 1 day, followed by immersion into a 0.1 mM sodium nitrate solution in propylene glycol for at least three more days. This equilibration process, typically referred to as conditioning, replaces the anions originally present in the ion-exchange membrane with nitrate and permits some swelling of the ion exchanger with the solvent. Subsequent storage for up to 3 weeks in propylene glycol showed no degradation of the membranes' performance.

Electrodes with conditioned sensing membranes were then used to determine the nitrate response in propylene glycol at ambient temperatures before and after exposure to 150 °C. Before any high-temperature exposure, the electrodes with all three types of membranes gave similar results, showing a decrease of the measured potential, emf, of approximately 50 mV per 10-fold increase in the activity of nitrate. Next, the electrodes were placed in 0.1 mM sodium nitrate in propylene glycol, which was then heated to 150 °C for 5 h. Note that the boiling point of propylene glycol is 188 °C, which is not only above the boiling point of water, but it is also well above the reaction temperature for the nanoparticle synthesis used in this work. After the electrodes were allowed to cool to ambient temperature, the nitrate response was measured again. Only the AHO membranes (made of polystyrene with quaternary ammonium ionic sites and cross-linked with divinylbenzene) exhibited consistent nitrate responses after the exposure to 150 °C. In contrast, the electrodes with the FAB and AMI membranes were prone to failure after heating, often failing to give any response to nitrate.

In an attempt to better understand the different behavior of the three types of ion-exchange membranes, they were characterized with differential scanning calorimetry (DSC; for DSC traces, see Supporting Information). Surprisingly, the AHO membranes exhibited, with a phase transition around 121 °C, the largest response to temperature at ≤150 °C. The shift of this transition from 125.6−130.5 °C during the first segment to 114.9−127.5 °C in subsequent heating segments is likely due to annealing of the polymer.[52] Importantly, there was an almost perfect overlap of the DSCs of the second and third heating cycle, which shows that although the AHO membranes undergo a transition in every heating cycle, repeated heating does not degrade these membranes.

Since only the AHO membranes performed well in potentiometric measurements after exposure to 150 °C, they were the only membranes further investigated. Therefore, let us briefly revisit the potentiometric

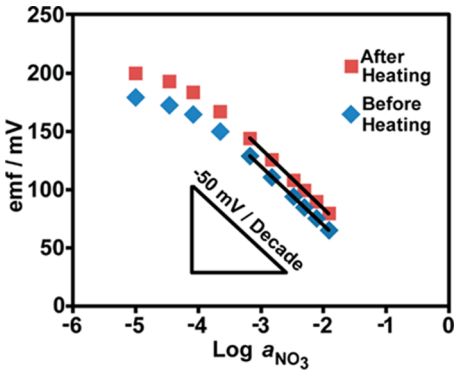

Figure 1. ISE with an AHO ion-exchange membrane: Emf response to nitrate in propylene glycol at 22 °C, before and after heating at 150 °C for 5 h.

response slope observed with the AHO membranes. Note that the Debye−Hückel limiting law was used to determine the activity of nitrate:[53]

$$\ln(\gamma_i) = -\frac{z_i^2 q^3 N_A^{1/2}}{4\pi(\varepsilon_r \varepsilon_0 k_B T)^{3/2}} \sqrt{\frac{I}{2}}$$

where z_i is the charge of the ion species i, q is the elementary charge, N_A is Avogadro's number, ε_r is the relative permittivity (dielectric constant) of the solvent (32 at 20 °C for propylene glycol), ε_0 is the permittivity of free space, k_B is Boltzmann's constant, and I is the ionic strength of the solution. With the use of this formalism, the average response slopes for the AHO membranes before and after heating were calculated to be −50.8 ± 0.2 and −50.3 ± 0.3 mV/decade change in the activity of nitrate, respectively (Figure 1). These values are close to but somewhat lower than the theoretical response slope of −58.1 mV/decade for 20 °C, as predicted by the Nernst equation:

$$\text{emf} = E^\circ + \frac{2.303RT}{z_i F} \log a_i$$

where E° is the calibration curve intercept, z_i is the charge of the measured ion, and R, T, and F are the gas constant, temperature, and Faraday's constant, respectively. This may be attributed to several factors. A more accurate assessment of the activity coefficients, for example, by using the extended Debye−Hückel equation, could possibly improve the slope. However, such calculations for solutions made from propylene glycol are not possible without considerable work outside of the scope of this project. Moreover, contributing to the slightly smaller than expected slope may be the liquid junction potential between the reference electrode and the sample solutions, which is expected to be small but may differ somewhat for the different points of the calibration curve.[54] Corrections of the measured emf for changes in the liquid junction potential[55,56] were not attempted because ion mobilities in propylene glycol are also not known from the literature. Important for this work is the fact that the response slopes are

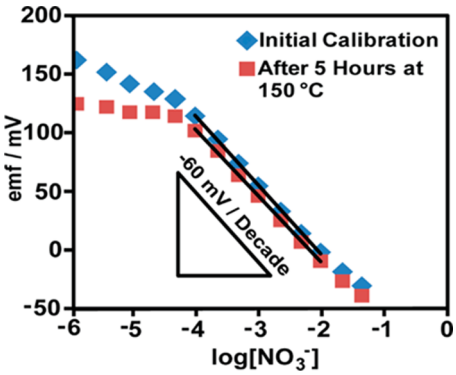

Figure 2. Nitrate response of an ISE with an AHO ion-exchange membrane at 150 °C in propylene glycol: Initial response and response after 5 h at 150 °C.

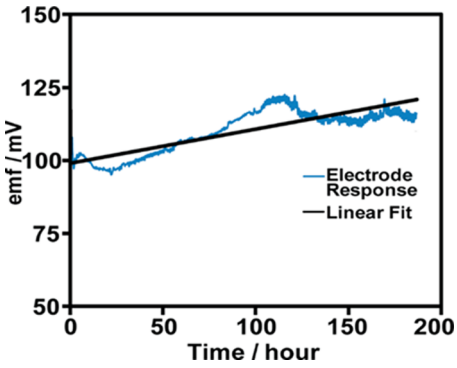

Figure 3. AHO membrane nitrate sensor response at 150 °C for over 180 h.

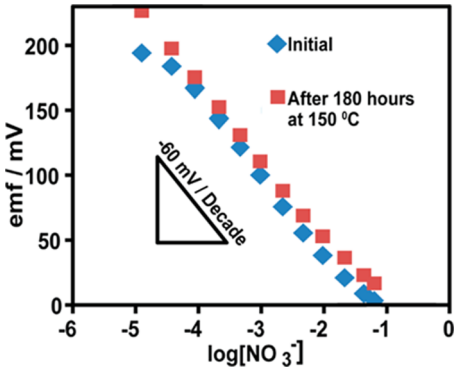

Figure 4. Response of AHO membrane sensor to nitrate in propylene glycol at 150 °C: Initial response curve and response curve after 180 h of heating.

reproducible, show an acceptable linear range, and are unaffected by heating for 5 h in propylene glycol. This shows that the AHO membranes can successfully measure in propylene glycol and can survive being heated to 150 °C. It should be noted that, after a concentration change, it takes approximately 2 min for the measured emf to stabilize. Because these electrodes respond much faster at higher temperatures (see below), it appears likely that this comparatively long response time is explained predominantly by the high viscosity of propylene glycol at ambient temperature.

High Temperature Measurements. ISEs equipped with AHO sensing membranes were also used to directly measure the nitrate activity in propylene glycol at 150 °C by stepwise addition of aliquots of $NaNO_3$ in propylene glycol (Figure 2). The average slope of the nitrate response at this temperature was -60 ± 1 mV/decade change in the concentration of nitrate. Activity coefficients for nitrate in propylene glycol were not calculated because that would require knowledge of the dielectric constant of propylene glycol at 150 °C, which is not readily available. The limit of nitrate detection was determined to be 18 ± 6 μM, with a linear range from 0.1 mM to 10 mM. Within the linear response range, the emf response was very stable, with a drift of the measured emf of less than 0.1 mV/min. The response time in this range was with less than 10 s (see the Supporting Information) much smaller than at ambient temperature, which is likely due to the large decrease in the viscosity of propylene glycol at 150 °C.[13]

To determine whether the electrochemical cell consisting of a reference electrode, the propylene glycol solution, and an ISE with an AHO membrane could function for several hours at 150 °C, the whole cell was heated to 150 °C, and a calibration curve for the nitrate response was measured. At this point, the solution was replaced with a propylene glycol solution containing 0.1 mM sodium nitrate, and the electrochemical cell was heated to 150 °C for 5 h, after which the nitrate calibration curve was once again measured at 150 °C (Figure 2). The comparison of the response curves before and after heating shows only a minor loss of the limit of detection (16 μM to 50 μM). Importantly, the linear range was unchanged, and the change in E° was only 1.8 ± 2.7 mV. This demonstrates that the sensor can function for the duration of a typical nanoparticle synthesis with minimal performance changes over the course of the experiment.

Lifetime. To determine the lifetime of the electrodes at high temperatures, the emf was monitored continuously for 180 h at 150 °C in a stirred propylene glycol solution containing 1.0 mM sodium nitrate solution (Figure 3). The electrode showed only a small overall drift (0.0019 mV/min), with a standard deviation of 7.5 mV from the average value over the course of the entire experiment. The nitrate response before and after 180 h at 150 °C also showed little change, as shown in Figure 4. This illustrates that the AHO membranes have good thermal stability and can function at high temperatures for long periods of time.

To test the effects of repeated heating and cooling, an electrochemical cell was set up using an ISE with an AHO ion-exchange membrane and a reference electrode in a 1.0 mM sodium nitrate solution in propylene glycol. The temperature was switched several times in 30 min intervals between room temperature (22 °C) and 150 °C. The sensors' average response for three

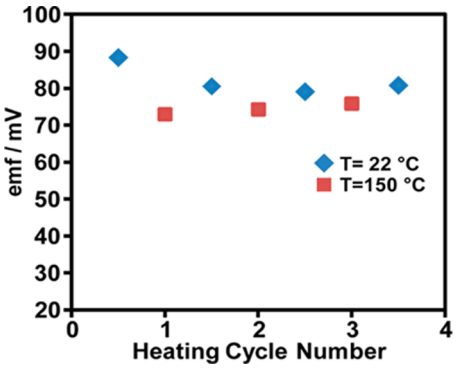

Figure 5. Average emf response of ISEs with an AHO ion-exchange membrane after multiple heating/cooling cycles between 22 and 150 °C.

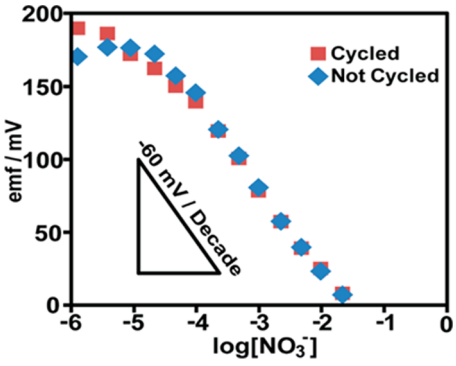

Figure 6. Calibration curve for nitrate ISEs with an AHO ion-exchange membrane at 150 °C before and after temperature cycling.

cycles is shown in Figure 5. The average value of the emf at 150 °C was highly reproducible, with a standard deviation of only 1.0 mV between heating cycles. There was a change in the emf at room temperature after the first heating cycle (approximately 10 mV), compared to the emf before heating. However, there was little to no change thereafter, with a standard deviation of 0.9 mV between measurements at room temperature after subsequent heat exposures, which is consistent with the results of the DSC. Moreover, the calibration curve for nitrate at 150 °C after the cycling of the temperature showed little change compared to the response of the electrodes that had only been heated to 150 °C once (Figure 6).

Selectivities. Before the selectivity of ISEs equipped with an AHO ion-exchange membrane were determined, the response of these electrodes to the anions of interest was measured in propylene glycol at 150 °C. Both the fixed primary ion method and the separate solution methods were used to determine selectivity coefficients,[57] and they showed good agreement between one another (see Table 1; for response slopes values, see the Supporting Information), suggesting that these values are unbiased manifestations of the thermodynamic ion-exchange properties of the AHO ion-exchange membranes. The coefficients represent

TABLE 1. Selectivity Coefficients of the ISE for Chloride and Acetate, As Measured with the Separate Solution Method (SSM) and the Fixed Primary Ion Method (FPIM) with Respect to Nitrate

$\mathrm{Log}K_{NO_3^-,J}^{pot}$	SSM	FPIM
Cl^-	0.29 ± 0.05	0.17 ± 0.16
NO_2^-	−0.03 ± 0.03	0.02 ± 0.06
OAc^-	−0.11 ± 0.07	−0.09 ± 0.24

a much reduced selectivity, compared to classical solvent−polymeric ionophore-free ion-exchange membranes.[58] As expected, they are similar in range to those determined in aqueous solutions for other types of hydrophilic high-capacity ion-exchange membranes[42] and are comparable to analogous selectivity ranges for ion-exchange resins.[38] The rather narrow range of selectivity coefficients suggests that these ISEs are best used when the concentration of the anion of interest is much higher than the concentration of other anions in solution and would not be useful in a system with a high concentration of background electrolyte. While this may appear to be a drawback, it is worthwhile to remember that, unlike in the case of classical solvent polymeric ionophore-free ion-exchange membranes, highly lipophilic ions at low to intermediate concentrations will not cause substantial interference.[42]

Measurements During Nanoparticle Synthesis. Having confirmed the suitability of ISEs with AHO ion-exchange membranes for measurements at 150 °C in propylene glycol, these electrodes were used for *in situ* measurements in the polyol synthesis of nanoparticles. First, an ISE was calibrated at 150 °C by additions of $NaNO_3$ aliquots into a propylene glycol solution containing 1.11 g/L polyvinylpyrrolidone (PVP), which corresponds to 10 mM of the PVP monomer. The ISE was then used to monitor the synthesis of copper nanoparticles, which was performed by using a modified literature procedure reported for the synthesis of Ag nanoparticles.[13,17] The electrodes were placed in propylene glycol containing PVP, the solution was heated to 150 °C, and then $Cu(NO_3)_2$ in propylene glycol was added at a rate of 1 mL/s. The potential of the electrochemical cell was monitored over the course of the whole reaction time, and aliquots were taken for *ex situ* analysis by ion chromatography and colorimetric analysis. During the course of the copper nanoparticle synthesis, the light-blue solution changed, initially, to a blue suspension, which later turned green and, finally, brown/red, consistent with earlier reports of copper nanoparticle synthesis.[15] The synthesis of silver nanoparticles was performed similarly by the addition of 110 mM $AgNO_3$ over 20 min and ending the reaction after 1 h. In this case, the initially colorless solution first turned yellow and then turned into a suspension, whose appearance was first yellow but changed later into yellowish gray, again, consistent with earlier observations.[14]

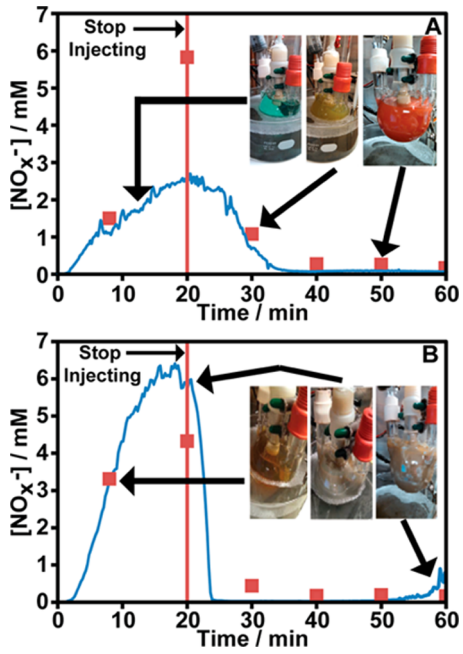

Figure 7. Concentration of NO_X^- as determined by potentiometry with ion-exchange membranes (blue line) and ion-exchange chromatography (red squares) during a typical (A) copper nanoparticle synthesis, and (B) silver nanoparticle synthesis (both at 150 °C). Insets: Photographs of reaction flask showing the colors of the suspensions as the reactions progressed.

As shown in Figure 7, the ISEs were able to measure the concentration of anions throughout the course of both the copper and silver nanoparticle syntheses. As discussed below, this led us to discover the formation of NO_2^- in these reactions. Note that the calibration curve for $NaNO_3$ described above could be used without modification to determine the concentration of NO_X^- because the electrodes were found to respond nearly equally to NO_3^- and NO_2^- ($K_{NO_3^-,NO_2^-}^{pot} \approx 1$). Therefore, in the context of the nanoparticle syntheses, we will refer from hereon to potentiometric measurements of NO_x^-.

In both reactions, the highest detected NO_X^- concentration was much lower than would be expected based on the amount of nitrate injected. While the concentration of NO_X^- at the end of the metal nitrate addition should have reached 10 mM in both the copper and the silver nanoparticle synthesis, the highest detected values were 2.5 ± 0.44 mM for the copper reaction and 6.3 ± 0.33 mM for the silver reaction. Evidently, in both cases nitrate decomposition began quickly. The measured NO_X^- concentration increased gradually but slower than predicted from the addition rate. Also, soon after the injection was stopped, the NO_X^- concentrations began to fall. For the copper reaction, the NO_X^- concentration fell to 0.1 mM approximately 12 min after the injection was stopped and then continued to slowly decrease down to a minimum of 0.040 mM. Note that the blue-to-green change in color in the copper nanoparticle synthesis occurred between 30 and 40 min after the start of the reaction, and the change from green to red occurred after 50 min. In the silver reaction, the drop in NO_X^- concentration is much steeper, reaching 0.1 mM in less than 4 min, followed by a further but slower decrease in NO_X^- concentration down to a value nearly 2 orders of magnitude lower than the maximum concentration. In the silver reaction, a yellow color appeared almost immediately and turned to a yellowish gray after about 15 min, when the NO_X^- concentration also leveled off. Between 10 and 25 min, gas bubbles could be seen vigorously forming in the reaction mixture.

We found that it is important to make sure that the electrode membrane does not become covered with bubbles, as this can affect the potential of the electrodes and cause errors in determining the ion concentration. To avoid this problem, the lip on the cap of the electrode was reduced in size, and the electrode was inserted into the reaction solution at an angle of approximately 45° with respect to the horizontal level of the solution to prevent bubbles from being trapped on the surface of the electrode membrane (see Supporting Information). For both reactions, the low concentration of detected anions at the end of the reaction suggests that the majority of NO_X^- ions were either bound to the surface of the nanoparticles or were converted into decomposition products such as NO or NO_2 gas. However, the distinctive color of NO_2 gas was not observed in the gas leaving the reaction flask.

A comparison of the results of the colorimetric analysis, the ion chromatography, and the results obtained by using the potentiometric sensor is shown in Figure 8 and Table S2. Surprisingly, the colorimetric analysis and the ion chromatography showed that nitrite was formed during the reaction. We have not been able to find in the literature any mention of nitrite formation during this type of nanoparticle synthesis. In a control experiment, propylene glycol solutions with PVP and sodium nitrate, but no transition metal nitrate, were heated to 150 °C. Colorimetric analysis and ion chromatography showed no evidence for the reduction of nitrate to nitrite. This demonstrates that the presence of copper or silver is necessary for the nitrate reduction to occur.

There are several possibilities on what is causing the reduction of nitrate. One possibility is that the NPs are being oxidized. Another possibility is that the NP surface catalyzes the reduction of nitrate by aldehydes that are formed in heated propylene glycol (reducing agents that also have been proposed to be relevant in the formation of nanoparticles).[16] Further study will be needed to clarify the mechanism of nitrate reduction.

In the copper reaction, the NO_X^- concentration determined by the potentiometric sensor varied substantially from that of the total concentration of nitrate and nitrite as determined by the colorimetric method

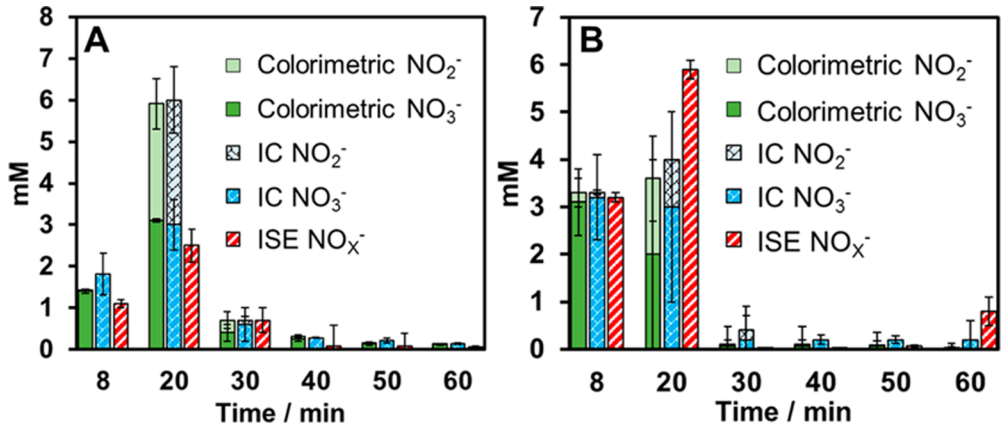

Figure 8. Comparison of average NO_X^- concentrations during three (A) copper and (B) silver nanoparticle syntheses, as determined by the electrochemical nitrate sensor, ion chromatography, and colorimetric analysis. Concentration values are cumulative.

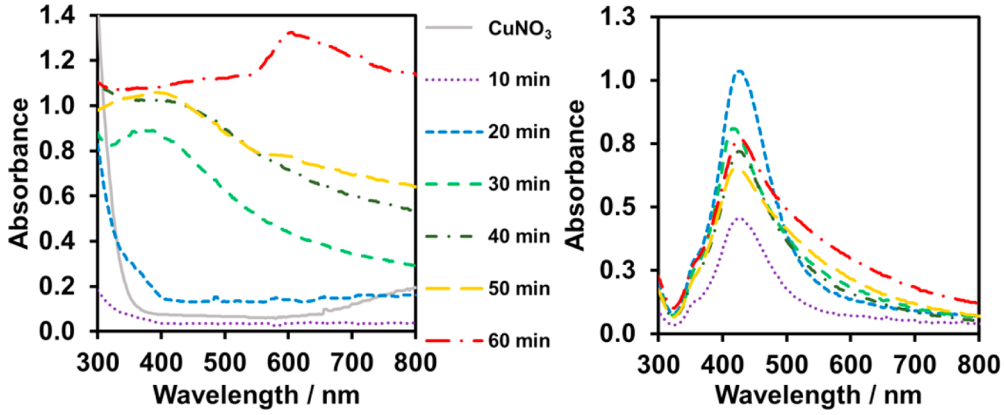

Figure 9. Absorbance spectra of samples from the syntheses of copper (right) and silver nanoparticles (left).

and by ion chromatography. However, the trend of decreasing NO_X^- concentration over time after the stop of the $Cu(NO_3)_2$ injection is apparent in the data from all three methods of analysis. The differences between the data from the *in situ* and the *ex situ* methods is likely explained by NO_X^- binding to the copper surface of the nanoparticles. Indeed, nitrate binding to Cu(100) has been reported in the literature, and density functional theory calculations suggest that this anion binds strongly (−249 kJ/mol) in a bidentate fashion (through two oxygen atoms) to the copper surface.[59] This is consistent with near quantitative binding, allowing for a high surface coverage. Indeed, binding of NO_3^- to Cu nanoparticles in systems containing 1-butyl-3-methylimidazolium nitrate has been shown using X-ray photoelectron spectroscopy.[60] While the potentiometric method measures only the NO_X^- anions that are freely dissolved but not those adsorbed to nanoparticles, the two *ex situ* techniques are based on a workup that displaced NO_X^- from the nanoparticle surface and measured the total NO_X^- in the reaction suspension. The ion chromatography, colorimetric, and potentiometric data for the silver reaction match much better, suggesting little binding of NO_X^- onto silver nanoparticles. Note that the *ex situ* methods also suffered from the error introduced by the time it takes one to remove and quench the sampled aliquot. In particular, the standard deviation for the NO_X^- concentration as determined with *ex situ* techniques is very large for sampling during the time range in which the NO_X^- concentration drops sharply in the silver reaction, which is right after injection has ceased (20 min). This showcases the advantages of *in situ* measurements to monitor polyol synthesis reactions.

UV−visible spectra were taken of the samples from both the copper and silver nanoparticle reactions, as shown in Figure 9. For the silver nanoparticle reaction, the maximum absorbance for each sample was at 422 nm. There is increased absorbance at wavelengths higher than 422 nm in samples from the second half of the reaction, which suggests that larger particles are forming and that the particle size is becoming more disperse. Transmission Electron Microscopy (TEM) images of nanoparticles taken from the end of the reaction confirmed the average size of the particles to be 35 ± 14 nm (see Supporting Information for images). Small amounts of bars similar in width to that of the diameter nanoparticles were also observed. The obtained absorbance values match well for particles of this size as seen in the literature.[61] Energy-dispersive X-ray

spectroscopy (EDS) spectra conformed the identity of the particles as silver.

For the copper nanoparticle reaction, the UV spectra suggest small particles <10 nm in diameter at early times (absorbance at approximately 400 nm).[60] Their small size provides a large surface area for binding of nitrate, which explains in part the differences seen in between the nitrate concentrations determined with ISEs and with ion chromatography. After 50 min, there is an increase in the concentration of larger particles, as evidenced by the appearance of absorbance at 596 nm.[15] TEM of nanoparticles taken from the end of the reaction confirmed the average size of the particles to be 360 ± 12 nm (see Supporting Information for images), but small amounts of bars similar in width to that of the nanoparticles were also observed. EDS spectra conformed the identity of the particles as copper.

Reactions performed with and without immersion of the sensor and reference electrode into the reaction mixture showed very similar absorption spectra, with no significant changes in the absorbance maxima. This is not surprising as these electrodes do not contain metal surfaces, nor do they have sharp edges that would affect the nucleation of nanoparticles or permit leaching of any ions into the samples that are not already in the reaction solutions.

CONCLUSION

The new potentiometric sensors with a hydrophilic high-capacity ion-exchange membrane can be used to measure *in situ* under the harsh conditions of propylene glycol at 150 °C. Unlike many spectroscopic probes, the ISE can be applied in completely turbid solutions and, with proper design, it is also immune to error from the abundant bubbles that form in the synthesis of nanoparticles. The sensor has a long lifetime, as it is able to measure at 150 °C for over 180 h and survives several heating and cooling cycles, showing its suitability as a useful tool for *in situ* monitoring in nanoparticle synthesis. We used this sensor successfully to monitor the co-ion concentration in the synthesis of two types of nanoparticles. In both of them, a change in the nitrate concentration of almost 2 orders of magnitude was observed. Using colorimetric and ion chromatography measurements, we discovered that the reduction of nitrate to nitrite is an important process, and that NO_X^- species are bound to the copper nanoparticles. The changes in the concentration of nitrate during the nanoparticle synthesis raise the question whether the counterions of the metal precursor may have an effect on how quickly nanoparticles grow. The potentiometric sensors introduced here have promise to help answer questions of this type. Sensing of this type is not limited to the detection of anions, as cation-exchange membranes similar to the anion-exchange membranes used in this work exist.[38] Hydrophilic high-capacity ion exchange membranes are also suitable for ions of various sizes and shapes.[62] This suggests that similar sensors could be used to monitor a variety of other ions under similar conditions.

METHODS

Materials. Three types of ion-exchange membranes were used in this study: Fumasep FAB anion exchange membranes (a PEEK reinforced membrane, 0.13 mm thick, sold loaded with bromide as counterion, with a capacity of >1.3 mequiv/g, electrical resistance <1 Ω cm^2, and reported by the manufacturer to be functional at 80 °C, although under substantial swelling with water; Fumatech, Bietigheim-Bissingen, Germany),[49] SELEMION AHO anion exchange membranes (a polystyrene with quaternary ammonium ionic sites and cross-linked with divinylbenzene, 0.30 mm thick, loaded with bromide, with an electrical resistance of 20 Ω cm^2, and labeled by the manufacturer as suitable for use in hot water and in the presence of oxidants; AGC Engineering, Nakase, Japan),[50] and AMI-7001S anion exchange membranes (a gel polystyrene with quaternary ammonium ionic sites and cross-linked with divinylbenzene, 0.45 mm thick, loaded with chloride, with an ion exchange capacity of 1.3 ± 0.1 mequiv/g, electrical resistance <40 Ω cm^2, and the thermal stability was reported by the manufacturer to be 90 °C; Membrane International, Ringwood, NJ).[51] All ion exchangers were characterized by using differential scanning calorimetry on a TA Instruments Q1000 (New Castle, DE). The temperature was cycled from −20 to 200 °C, several times, with a scan rate of 10 °C/min. The AHO membrane was received in a solution and was rinsed with deionized water, blotted dry, and allowed to dry for 24 h under ambient conditions before DSC measurements. Experiments after drying these ion-exchange membranes under vacuum yielded nearly identical results. Propylene glycol (99%) was purchased from Sigma-Aldrich (St. Louis, MO), porous glass frits from Princeton Applied Research (Oak Ridge, TN), and polyvinylpyrrolidone (sold as Kollidon 30, M_w = 44 000−54 000) from BASF (Ludwigshafen, Rheinland-Pfaltz, Germany).

Assembly of the Ion-Selective Electrodes. Ion-exchange membranes where cut into 15 mm diameter disks, conditioned in propylene glycol containing different concentrations of $NaNO_3$ (see above), and then mounted into custom-machined electrode bodies made from polyether ether ketone (PEEK) using a silicone O-ring and a screw-on PEEK cap, as previously described in the literature.[63,64] See the Supporting Information for further details. All electrode components exposed to the sample solution were fabricated with rounded edges to reduce nanoparticle growth on the surface of the electrode. The electrode contained two inner liquid compartments: (i) the outer filling solution (0.1 mM sodium nitrate solution in propylene glycol), which was in direct contact with the sensing membrane, and (ii) a 0.1 mM sodium chloride solution in propylene glycol (referred to as the inner filling solution), into which a AgCl-coated Ag wire was inserted as the reference half-cell. A compartment to contain the inner filling solution and allow for a liquid junction between the two filling solutions was prepared by securing a plastic micropipette tip packed at the narrow end with cotton and sealed at the top with a septum. The thus prepared inner reference electrode was mounted from the top into the PEEK body, using Tygon tubing and Parafilm.

Assembly of the Reference Electrode. A custom-made double-junction reference electrode was equipped with a porous glass frit (Princeton Applied Research, Oak Ridge, TN) to separate the sample from the outer filling solution (propylene glycol saturated with KNO_3). A second porous glass frit separated the

outer filling solution from the inner filling solution (propylene glycol saturated with KCl and AgCl). A AgCl-coated Ag wire was inserted into the latter as an internal reference element (see Supporting Information).

Potentiometric Measurements. All calibration curves and nanoparticle syntheses were performed in solutions contained in a round-bottom flask with three necks, which were all stoppered with a rubber septum. The reference electrode and the ISE were inserted into the propylene glycol solution through two septa. The third septum was used to insert a temperature probe in order to add reagents with a syringe, and in the case of nanoparticle syntheses, to flush with nitrogen. For measurements at 150 °C, the reaction solution was heated with an oil bath on a hot plate connected to the temperature probe. Sensor calibrations were performed by the addition of aliquots of a propylene glycol solution of the sodium salt of the anion of interest. Selectivity coefficients were determined using the fixed primary ion method[57] and the separate solutions method, both at 150 °C. EMF Suite 1.03 software (Fluorous Innovations, Arden Hills, MN) was used with an EMF 16 potentiometer (Lawson Labs, Malvern, PA).

Copper and Silver Nanoparticle Synthesis. An ISE was placed into 200 mL of propylene glycol containing 0.122 g of PVP, and the solution was heated to 150 °C. Then, 20 mL of 55 mM $Cu(NO_3)_2$ or 110 mM of $AgNO_3$ in propylene glycol was added at a rate of 1 mL/s. The potential of the electrochemical cell was monitored over the course of the whole reaction time, which was 60 min. Over this time, six aliquots were taken for *ex situ* analyses by ion chromatography and by colorimetric analysis.

***Ex Situ* Colorimetric Analysis of Nitrate and Nitrite.** Samples for *ex situ* measurements of nitrate and nitrite concentrations in the silver nanoparticle synthesis solutions were collected periodically over the course of the reactions. All samples were diluted with water by a factor of 5 and frozen to quench any further reaction. For analysis, the samples were thawed and centrifuged. Colorimetric analysis at 520 nm was performed on the supernatant at the University of Minnesota Research Analytical Laboratory using a Lachet 8500 FIA spectrophotometer. The nitrite concentration was determined first, followed by reduction with cadmium to give the total nitrite and nitrate concentrations. The nitrate concentration was determined by difference.[65]

Ion Chromatography. Ion chromatography was performed with a Dionex Ion Pac AS11 column and a Dionex Anion Self-Regulating Suppressor ASRS-I with a suppression voltage of 300 mV, with 3 mM NaOH in a 1:4 propylene glycol/water mixture as the eluent.

UV–Vis Absorbance Spectroscopy. UV–vis spectroscopy was performed using a Hewlett-Packard 8452A diode array spectrophotometer.

Transmission Electron Microscopy (TEM) and Energy-Dispersive X-ray Spectroscopy (EDS). TEM images and EDS spectra were obtained on a FEI Tecnai T12 microscope operated at 120 kV and equipped with a LaB6 electron source. Images were recorded using a Gatan MSC794 CCD camera. Samples were prepared on a copper TEM grid. Particle size measurements were performed using ImageJ (version 1.8.0), an open source program written by Wayne Rasband at the U.S. National Institutes of Health.[66] A volume of 1 mL of sample was added to 5 mL of 2-propanol and then the mixture was centrifuged twice at 9000 rpm for 30 min. The nanoparticles were then washed twice with 5 mL of 2-propanol, resuspended in 2-propanol, dropped onto a TEM grid (holey carbon, 200 mesh, copper grid; SPI), and the solvent was then allowed to evaporate. The average particle size was determined by measuring the diameter of particles from several images taken from different sections of the sample.

Conflict of Interest: The authors declare no competing financial interest.

Acknowledgment. Part of this research was funded by Carestream Health. We thank United Science for the use of their ion chromatography system, and the University of Minnesota Research Analytical Laboratory for performing the colorimetric analysis.

Supporting Information Available: The Supporting Information is available free of charge on the ACS Publications website at DOI: 10.1021/acsnano.5b05170.

Details of the assembly of the reference and ion-selective electrode; effect of bubbles on the measured potential; DSCs of all ion exchangers; TEM images of silver and copper nanoparticles (PDF)

REFERENCES AND NOTES

1. Pradhan, N.; Pal, A.; Pal, T. Silver Nanoparticle Catalyzed Reduction of Aromatic Nitrocompounds. *Colloids Surf., A* **2002**, *196*, 247–257.
2. Kamat, P. V. Photophysical, Photochemical and Photocatalytic Aspects of Metal Nanoparticles. *J. Phys. Chem. B* **2002**, *106*, 7729–7744.
3. Li, Y.; Wu, Y.; Ong, B. S. Facile Synthesis of Silver Nanoparticles Useful for Fabrication of High-Conductivity Elements for Printed Electronics. *J. Am. Chem. Soc.* **2005**, *127*, 3266–3267.
4. Shipway, A. N.; Katz, E.; Willner, I. Nanoparticle Arrays on Surfaces for Electrical, Optical, and Sensor Aplications. *ChemPhysChem* **2000**, *1*, 18–52.
5. Michaels, A. M.; Jiang, J.; Brus, L. Ag Nanocrystal Junctions as the Site for Surface-Enhanced Raman Scattering of Single Rhodamine 6G Molecules. *J. Phys. Chem. B* **2000**, *104*, 11965–11971.
6. Maier, S. A.; Brongersma, M. L.; Kik, P. G.; Meltzer, S.; Requicha, A. A. G.; Atwater, H. A. Plasmonics-A Route to Nanoscale Optical Devices. *Adv. Mater.* **2001**, *13*, 1501–1505.
7. Magdassi, S.; Bassa, A.; Vinetsky, Y.; Kamyshny, A. Silver Nanoparticles as Pigments for Water-Based Ink-Jet Inks. *Chem. Mater.* **2003**, *15*, 2208–2217.
8. Rai, M.; Yadav, A.; Gade, A. Silver Nanoparticles as a New Generation of Antimicrobials. *Biotechnol. Adv.* **2009**, *27*, 76–83.
9. Lee, K.-S.; El-Sayed, M. A. Gold and Silver Nanoparticles in Sensing and Imaging: Sensitivity of Plasmon Response to Size, Shape, and Metal Composition. *J. Phys. Chem. B* **2006**, *110*, 19220–19225.
10. Magdassi, S.; Grouchko, M.; Kamyshny, A. Copper Nanoparticles for Printed Electronics: Routes Towards Achieving Oxidation Stability. *Materials* **2010**, *3*, 4626–4638.
11. Fievet, F.; Lagier, J. P.; Figlarz, M. Preparing Monodisperse Metal Powders in Micrometer and Submicrometer Sizes by the Polyol Process. *MRS Bull.* **1989**, *14*, 29–34.
12. Chokratanasombat, P.; Nisaratanaporn, E. Preparation of Ultrafine Copper Powders with Controllable Size *via* Polyol Process with Sodium Hydroxide Addition. *Eng. J.* **2012**, *16*, 39–46.
13. Park, K. H.; Im, S. H.; Park, O. O. The Size Control of Silver Nanocrystals with Different Polyols and Its Application to Low-Reflection Coating Materials. *Nanotechnology* **2011**, *22*, 045602.
14. Wiley, B.; Sun, Y.; Mayers, B.; Xia, Y. Shape-Controlled Synthesis of Metal Nanostructures: The Case of Silver. *Chem. - Eur. J.* **2005**, *11*, 454–463.
15. Jianfeng, Y.; Guisheng, Z.; Anming, H.; Zhou, Y. N. Preparation of PVP Coated Cu NPs and the Application for Low-Temperature Bonding. *J. Mater. Chem.* **2011**, *21*, 15981–15986.
16. Skrabalak, S. E.; Wiley, B. J.; Kim, M.; Formo, E. V.; Xia, Y. On the Polyol Synthesis of Silver Nanostructures: Glycolaldehyde as a Reducing Agent. *Nano Lett.* **2008**, *8*, 2077–2081.
17. Zhang, L.; Wang, Y.; Tong, L.; Xia, Y. Seed-Mediated Synthesis of Silver Nanocrystals with Controlled Sizes and Shapes in Droplet Microreactors Separated by Air. *Langmuir* **2013**, *29*, 15719–15725.
18. Miyamoto, R. *Silver Wire and Its Manufacture by Reduction*, Japanese Laid Open Patent Publication 2008-190006, Aug. 21, **2008**.
19. Zhang, Q.; Li, W.; Moran, C.; Zeng, J.; Chen, J.; Wen, L.-P. W.; Xia, Y. Seed-Mediated Synthesis of Ag Nanocubes with

Controllable Edge Lengths in the Range of 30−200 nm and Comparison of Their Optical Properties. *J. Am. Chem. Soc.* **2010**, *132*, 11372–11378.
20. Habas, S.; Lee, H.; Radmilovic, V.; Somorjai, G. A.; Yang, P. Shaping Binary Metal Nanocrystals Through Epitaxial Seeded Growth. *Nat. Mater.* **2007**, *6*, 692–697.
21. Nandanwar, S. U.; Chakraborty, M.; Mukhopadhyay, S.; Shenoy, K. T. Stability of Ruthenium Nanoparticles Synthesized by Solvothermal Method. *Cryst. Res. Technol.* **2011**, *46*, 393–399.
22. Donnabelle, M. L. B. Syntheses of Metallic Cobalt Nanoparticles and Nanowires by Electroless Deposition. Ph.D. Thesis [Online], Kyoto University, September 2011. http://repository.kulib.kyoto-u.ac.jp/dspace/bitstream/2433/151979/2/D_Mary%20Donnabelle%20Lirio%20Balela.pdf (accessed September 12, 2015).
23. Balela, M. D. L.; Yagi, S.; Lockman, Z.; Aziz, A.; Amorsolo, A. V. J.; Matsubara, E. Electroless Deposition of Ferromagnetic Cobalt Nanoparticles in Propylene Glycol. *J. Electrochem. Soc.* **2009**, *156*, E139–E142.
24. Steinfeldt, N. In Situ Monitoring of Pt Nanoparticle Formation in Ethylene Glycol Solution by SAXS-Influence of the NaOH to Pt Ratio. *Langmuir* **2012**, *28*, 13072–13079.
25. Boita, J.; Nicolao, L.; Alves, M. C. M.; Jonder, M. Observing Pt Nanoparticle Formation at the Atomic Level During Polyol Synthesis. *Phys. Chem. Chem. Phys.* **2014**, *16*, 17640–17647.
26. Mowery, K. A.; Schoenfisch, M. H.; Baliga, N.; Wahr, J. A.; Meyerhoff, M. E. More Biocompatible Electrochemical Sensors Using Nitric Oxide Release Polymers. *Electroanalysis* **1999**, *11*, 681–686.
27. De Beer, D. Potentiometric Microsensors for In Situ Measurements in Aquatic Environments. *IUPAC Ser. Anal. Phys. Chem. Environ. Syst.* **2000**, *6*, 161–194.
28. Maurer-Jones, M. A.; Mousavi, M. P. S.; Chen, L. D.; Bühlmann, P.; Haynes, C. L. Characterization of Silver Ion Dissolution from Silver Nanoparticles Using Fluorous-Phase Ion-Selective Electrodes and Assessment of Resultant Toxicity to Shewanella Oneidensis. *Chem. Sci.* **2013**, *4*, 2564–2572.
29. Arvand, M.; Asadollahzadeh, S. A. Ion-Selective Electrode for Aluminum Determination in Pharmaceutical Substances, Tea Leaves and Water Samples. *Talanta* **2008**, *75*, 1046–1054.
30. Kakabadse, G. J.; Al-Aziz, M.; Al-Yawer, N. F. N.; Kaklugin, P.; Karim, M. R. O.; Perry, R.; Tipping, A. E.; Wake, P. Recent Advances in Direct Potentiometry in Organic and Mixed Solvents. *Port. Electrochim. Acta* **1988**, *6*, 5–25.
31. Jain, A.; Gupta, V. K.; Singh, R.; Khurana, U.; Singh, L. P. Nickel(II)-Selective Sensors Based on Heterogeneous Membranes of Macrocyclic Compounds. *Sens. Actuators, B* **1996**, *40*, 15–20.
32. Hu, M.; Cui, R.; Li, S.-N.; Jiang, Y.; Xia, S. P. Determination of Activity Coefficients for Cesium Chloride in Methanol-Water and Ethanol-Water Mixed Solvents by Electromotive Force Measurements at 298.15 K. *J. Chem. Eng. Data* **2007**, *52*, 357–362.
33. Durst, R. A.; Branscomb, L. M.; Stans, M. H. In *Ion-Selective Electrodes*, Symposium on Ion-Selective Electrodes, Gaithersburg, M. D., Durst, R. A., Eds.; National Bureau of Standards: Gaithersburg, MD, 1969; p 425.
34. Ibupoto, Z. H.; Khun, K.; Willander, M. A Selective Iodide Ion Sensor Electrode Based on Functionalized ZnO Nanotubes. *Sensors* **2013**, *13*, 1984–1997.
35. Chumbimuni-Torres, K. Y.; Bakker, E.; Wang, J. Real-Time Probing of the Growth Dynamics of Nanoparticles Using Potentiometric Ion-Selective Electrodes. *Electrochem. Commun.* **2009**, *11*, 1964–1967.
36. Li, N.; Guiver, M. D. Ion Transport by Nanochannels in Ion-Containing Aromatic Copolymers. *Macromolecules* **2014**, *47*, 2175–2198.
37. Adams, B. A.; Holmes, E. L. Method of and Means For Effecting Anionic Exchanges in Solutions. U.S. Patent 2,151,883, Mar. 28,1939.
38. Helfferich, F. *Ion Exchange*. Unabridged Dover ed.; Dover: Mineola, N.Y., 1995; p 623.
39. Kressman, T. R. E. Measurement of Ionic Activities in Solution with Solution with Electrodes Containing Ion-Exchange-Resin Membranes. *J. Appl. Chem.* **1954**, *4*, 123–131.
40. Wyllie, M. R. J.; Patnode, H. W. The Development of Membranes Prepared from Artificial Cation-Exchange Materials with Particular Reference to the Determination of Sodium-Ion Activities. *J. Phys. Colloid Chem.* **1950**, *54*, 204–227.
41. Bergin, M. J.; Heyn, A. H. A. Electrochemical Behavior of Cation Exchange Membranes in Liquid Ammonia. *J. Am. Chem. Soc.* **1954**, *76*, 4765–4769.
42. Grygolowicz-Pawlak, E.; Crespo, G. A.; Afshar, M. G.; Mistlberger, G.; Bakker, E. Potentiometric Sensors with Ion-Exchange Donnan Exclusion Membranes. *Anal. Chem.* **2013**, *85*, 6208–6212.
43. Titvinidze, G.; Kreuer, K.-D.; Schuster, M.; de Araujo, C. C.; Melchior, J. P.; Meyer, W. H. Proton Conducting Phase-Separated Multiblock Copolymers with Sulfonated Poly(phenylene sulfone) Blocks for Electrochemical Applications: Preparation, Morphology, Hydration Behavior, and Transport. *Adv. Funct. Mater.* **2012**, *22*, 4456–4470.
44. Schmidt-Rohr, K.; Chen, Q. Parallel Cylindrical Water Nanochannels in Nafion Fuel-cell Membranes. *Nat. Mater.* **2008**, *7*, 75–83.
45. Kong, X.; Schmidt-Rohr, K. Water-Polymer Interfacial Area in Nafion: Comparison with Structural Models. *Polymer* **2011**, *52*, 1971–1974.
46. Jagerszki, G.; Takacs, A.; Bitter, I.; Gyurcsanyi, R. E. Solid-State Ion Channels for Potentiometric Sensing. *Angew. Chem., Int. Ed.* **2011**, *50*, 1656–1659.
47. Makra, I.; Jagerazki, G.; Bitter, I.; Gyurcsanyi, R. E. Nernst−Planck/Poisson Model for the Potential Response of Permselective Gold Nanopores. *Electrochim. Acta* **2012**, *73*, 70–77.
48. Boswell, P. G.; Bühlmann, P. Fluorous Bulk Membranes for Potentiometric Sensors with Wide Selectivity Ranges: Observation of Exceptionally Strong Ion Pair Formation. *J. Am. Chem. Soc.* **2005**, *127*, 8958–8959.
49. Fumatech, Technical Data Sheet - Fumasep FAB. http://www.fumatech.com/NR/rdonlyres/0351A53E-568D-4BB9-A0DA-A57848AA1B2D/0/fumasepFAB.pdf (accessed July 2, 2015).
50. AGC Engineering. Selemion Ion Exchange Membranes. http://www.selemion.com/SELC.pdf (accessed July 2, 2015).
51. Membrane International, AMI-7001 Anion Exchange Membranes Technical Specifications. http://www.membranesinternational.com/tech-ami.htm (accessed July 2, 2015).
52. Hiemenz, P. C.; Lodge, T. P. *Polymer Chemistry*, 2 ed.; CRC Press: Boca Raton, FL, 2007; p 585.
53. Bockris, J. O. M.; Reddy, A. K. N. *Modern Electrochemistry 1, Ionics*, 2 ed.; Plenum Press: New York, NY, 1998; p 767.
54. Mousavi, M. P. S.; Bühlmann, P. Reference Electrodes with Salt Bridges Contained in Nanoporous Glass: An Underappreciated Source of Error. *Anal. Chem.* **2013**, *85*, 8895–8901.
55. Bard, A. J.; Faulkner, L. R. *Electrochemical Methods: Fundamentals and Applications*, 2 ed.; Wiley: New York, NY, 2001; p 833.
56. Morf, W. E. *The Principles of Ion-selective Electrodes and of Membrane Transport*; Elsevier: New York, NY, 1981.
57. Bakker, E.; Pretsch, E.; Bühlmann, P. Selectivity of Potentiometric Ion Sensors. *Anal. Chem.* **2000**, *72*, 1127–1133.
58. Bühlmann, P. P.; Bakker, E. Carrier-Based Ion-Selective Electrodes and Bulk Optodes. 2. Ionophores for Potentiometric and Optical Sensors. *Chem. Rev.* **1998**, *98*, 1593–1687.
59. Bae, S.-E.; Stewart, K. L.; Gewirth, A. A. Nitrate Adsorption and Reduction on Cu(100) in Acidic Solution. *J. Am. Chem. Soc.* **2007**, *129*, 10171–10180.
60. Hong, G. H.; Kang, S. W. Synthesis of Monodisperse Copper Nanoparticles by Utilizing 1-Butyl-3-methylimidazolium Nitrate and Its Role as Counteranion in Ionic Liquid in the Formation of Nanoparticles. *Ind. Eng. Chem. Res.* **2013**, *52*, 794–797.

61. Agnihotri, S.; Mukherji, S.; Mukherji, S. Size-controlled silver nanoparticles synthesized over the range 5−100 nm using the same protocol and their antibacterial efficacy. *RSC Adv.* **2014**, *4*, 3974–3983.
62. Ogawara, S.; Carey, J. L., III; Zou, X. Y.; Bühlmann, P. Donnan Failure of Ion-Selective Electrodes with Hydrophilic High-Capacity Ion-Exchanger Membranes. *ACS Sensors*, DOI: 10.1021/acssensors.5b00128.
63. Boswell, P. G.; Anfang, A. C.; Bühlmann, P. Preparation of a Highly Fluorophilic Phosphonium Salt and Its Use in a Fluorous Anion-Exchanger Membrane with High Selectivity for Perfluorinated Acids. *J. Fluorine Chem.* **2008**, *129*, 961–967.
64. Chen, L. D.; Lai, C.-Z.; Granda, L. P.; Fierke, M. A.; Mandal, D.; Stein, A.; Gladysz, J. A.; Bühlmann, P. Fluorous Membrane Ion-Selective Electrodes for Perfluorinated Surfactants: Trace-Level Detection and In Situ Monitoring of Adsorption. *Anal. Chem.* **2013**, *85*, 7471–7477.
65. Wendt, K. *QuikChem. Method 10-107-04-1-A, Determination of Nitrate/Nitrite in Surface and Wastewaters by Flow Injection Analysis*; Lachat Instruments: Milwaukee, WI, 2000; pp 1−17.
66. Rasband, W. S. *ImageJ*, 1st ed.; U.S. National Institutes of Health: Bethesda, MD, 1997.